NANO LETTERS

pubs.acs.org/NanoLett

Three-Dimensional Morphology and Crystallography of Gold Nanorods

Hadas Katz-Boon,[†] Chris J. Rossouw,[‡] Matthew Weyland,[†,‡] Alison M. Funston,[§,||] Paul Mulvaney,[§] and Joanne Etheridge*[,†,‡]

Department of Materials Engineering and Monash Centre for Electron Microscopy, Monash University, Victoria 3800, Australia, and School of Chemistry and Bio21 Institute, University of Melbourne, Parkville, VIC, 3010, Australia

ABSTRACT We determine the three-dimensional shape, to within 1 nm resolution, of single-crystal gold nanorods grown in the presence of silver ions using electron tomography and thickness profile measurements. We find that, contrary to the current literature, the octagonal side-facets are sparsely packed atomic planes all belonging to the same symmetry-equivalent family, {0 5 12}. Furthermore, the rod ends terminate in a pyramid with slightly different facets, and each pyramid is connected to the sides by four small {0 5 12} "bridging" facets.

KEYWORDS Gold nanorods, gold nanostructure, crystal growth, electron microscopy, electron tomography, scanning transmission electron microscopy

Understanding the mechanisms that determine crystal morphology is a major challenge in materials science.[1−4] Since the ground-breaking demonstration of nanocrystal shape control via surfactant templating,[5] gold nanorods have become the model system for understanding the growth of highly anisotropic, thermodynamically unexpected shapes.[6−9] These nanocrystals exhibit a variety of properties, which are exquisitely sensitive to shape, such as the optical response.[6,10,11] This has driven an intense effort over the past decade to understand and control their morphology.[7,12,13]

Theoretical studies of morphology[14] and current models of growth mechanisms[15,16] and shape transformations[17,18] are underpinned by a consensus that gold nanorods, grown in the presence of silver ions, are bound by the same facets as bulk gold, namely, the closely packed atomic planes: {1 0 0}, {1 1 0}, or {1 1 1} facets.[17,19−21] Specifically, the current morphological model describes these nanorods as an octagon formed by four {0 0 1} and four {0 1 1} side-facets and terminated by {1 0 0}, {1 1 0}, or {1 1 1} facets.[17,19−21] The growth of a rod-like shape implies that the rod ends grow at a faster rate than the sides,[20] so the identification of the rod end-facets and some of the side-facets as belonging to the same {1 0 0} family has been problematic. It is difficult to understand why the rods grow preferentially along only one of the three symmetry-equivalent ⟨1 0 0⟩ directions. Similarly, it is difficult to understand why the octagon should have side-facets belonging to symmetry-inequivalent atomic planes, which might be expected to have different surface energies.

Transmission electron microscopy (TEM) has been used to analyze nanorod morphology; however, it is difficult to obtain quantitative information about the specimen in the third dimension using conventional methods. For example, a single-atomic-resolution TEM image permits the identification of only a vector parallel to the facet plane. Images in several different projections are required to determine the orientation of the plane itself.[22,23]

Here we have undertaken an analysis of the three-dimensional shape (3D) and crystallography of gold nanorods using scanning transmission electron microscope (STEM) images acquired with a high-angle annular dark field (HAADF) detector. We have derived complementary 3D information from these images using two methods: HAADF-STEM tomography[24] and a novel HAADF-STEM "thickness profile" method.[25]

In HAADF-STEM, a focused electron beam is scanned across the specimen and at each point in the scan the electrons scattered to high angles are counted by an annular detector. The result is a two-dimensional (2D) "image" of intensity versus specimen position. The intensity has a monotonic dependence on specimen thickness (for thicknesses in the range considered here),[26−29] making it suitable for both the tomography and thickness profile methods.

HAADF-STEM tomography[24] enables the reconstruction of 3D shapes from a sequence of 2D images taken at different specimen orientations. Figure 1a−c shows a montage of images of the 3D morphology of a single gold nanorod, determined from a tomographic reconstruction and displayed as a surface rendering. (A movie is provided

* Corresponding author: joanne.etheridge@mcem.monash.edu.au.

[†] Department of Materials Engineering, Monash University.

[‡] Monash Centre for Electron Microscopy, Monash University.

[||] School of Chemistry, Monash University.

[§] University of Melbourne.

Received for review: 10/23/2010
Published on Web: 12/23/2010

DOI: 10.1021/nl103726k | *Nano Lett.* **2011,** *11,* 273–278

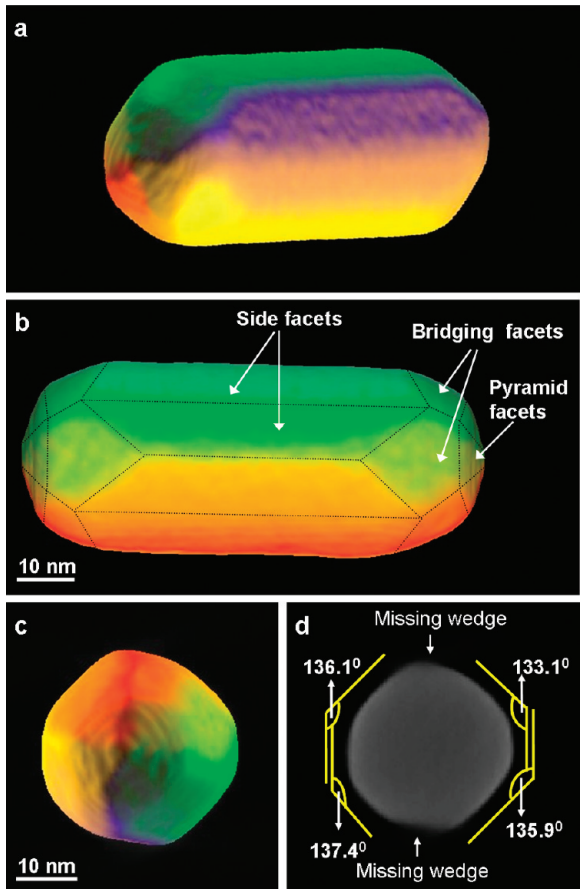

FIGURE 1. Montage of images visualizing the 3D shape of a gold nanorod determined from the tomographic reconstruction, viewed from a direction that shows (a) the end-cap, which has a pyramidal shape, (b) the bridging facets that connect the side facets with the end pyramid, (c) the nanorod viewed along the ⟨1 0 0⟩ direction, and (d) a cross-sectional slice taken from the middle of the rod showing that the cross-sectional shape is approximately octagonal, although the facet angles and side lengths differ slightly from a perfect octagon.

in the Supporting Information.) The image series was acquired using an ultrastable high-resolution instrument and operating environment[30] so that the reconstruction has a spatial resolution of better than 1 nm.[31]

It is possible to see that the shape of the nanorod, in a cross-section perpendicular to its long axis, is octagonal, as proposed in previous studies.[17,19−21] However, the angles between the side facets of the octagon are found to range from 133° to 137° (Figure 1d), and the widths of the side facets vary. It is also evident that the ends of the rods terminate in a pyramid shape, not the {0 0 1} plane, with additional bridging facets connecting the end pyramid to the side facets of the octagon. (The missing wedge in this reconstruction is a consequence of the inability to acquire images beyond the tilt range of the instrumentation and is unavoidable.)

We can determine the crystallographic orientation of the nanorod tomogram from zone axis images within the tilt series that exhibit 2D lattice fringes. This then enables us to identify the orientation of each of the facets, as detailed in Table 1. It is evident that both the side and bridging facets lie perpendicular to the ⟨0 1 1+√2⟩ direction, which bisects the angle between the ⟨011⟩ and ⟨001⟩ directions. The measurement uncertainty is within 3° for the side facets and 4° for the bridging facets. (For simplicity, hereafter we will refer to ⟨0 1 1+√2⟩ as ⟨0 5 12⟩, which lies within 0.1° of the ⟨0 1 1+√2⟩ direction.)

TABLE 1. Orientation of Nanorod Facets as Determined from the Tomogram

	surface normal			
facet	*u*	*v*	*w*	angle to ⟨0 5 12⟩ (deg)
side facets	0.02	−2.41	1	0.4
(uncertainty[a]	0.01	−2.43	1	0.3
from	0.03	2.27	1	1.3
tomogram	0.02	2.05	1	3.4
±3°)	−0.02	1	−2.39	0.5
	−0.02	1	−2.15	2.4
bridging facets	1	2.39	−0.06	1.3
(uncertainty[a]	1	2.27	0.05	1.6
from	1	−2.80	−0.01	3
tomogram ±4°)	1	−2.35	−0.12	2.7

	surface normal			
facet	*u*	*v*	*w*	angle to ⟨0 1 3⟩ (deg)
pyramid facets	2.86	1	0.06	1.4
(uncertainty[a]	2.63	1	0.10	3.1
from	−2.97	1	0.00	0.2
tomogram	−2.68	1	0.20	4.5
±5°)	3.03	−0.26	1	4.7

[a] As the area of the facet decreases, the measurement uncertainty increases.

The pyramid-facet orientation is slightly different from the side and bridging facets. Measurement of the pyramid facets is subject to greater error because of their small size and the proximity of the missing wedge. Nevertheless, all measurements indicate that the pyramid facets are closer to the {0 1 3} than the {0 5 12} family of planes, within experimental error.

In all cases, the intersection between facets is not sharp but rounded.

There is also a very weak contrast that suggests that the side facets and the end pyramid may have terraces parallel to ⟨0 0 1⟩. However, we emphasize that this detail is at the very limit of the resolution of this technique, and we cannot be confident of this observation.

To refine the facet orientation further and determine its generality, we developed a novel method[25] for converting a single HAADF-STEM image into a thickness profile image, where each pixel in the image gives the thickness of the specimen at that position. Once established, this method is quick (unlike tomography), enabling large numbers of nanorods to be analyzed so that any variation in nanorod morphology can be detected and measured.

DOI: 10.1021/nl103726k | *Nano Lett.* **2011,** *11,* 273–278

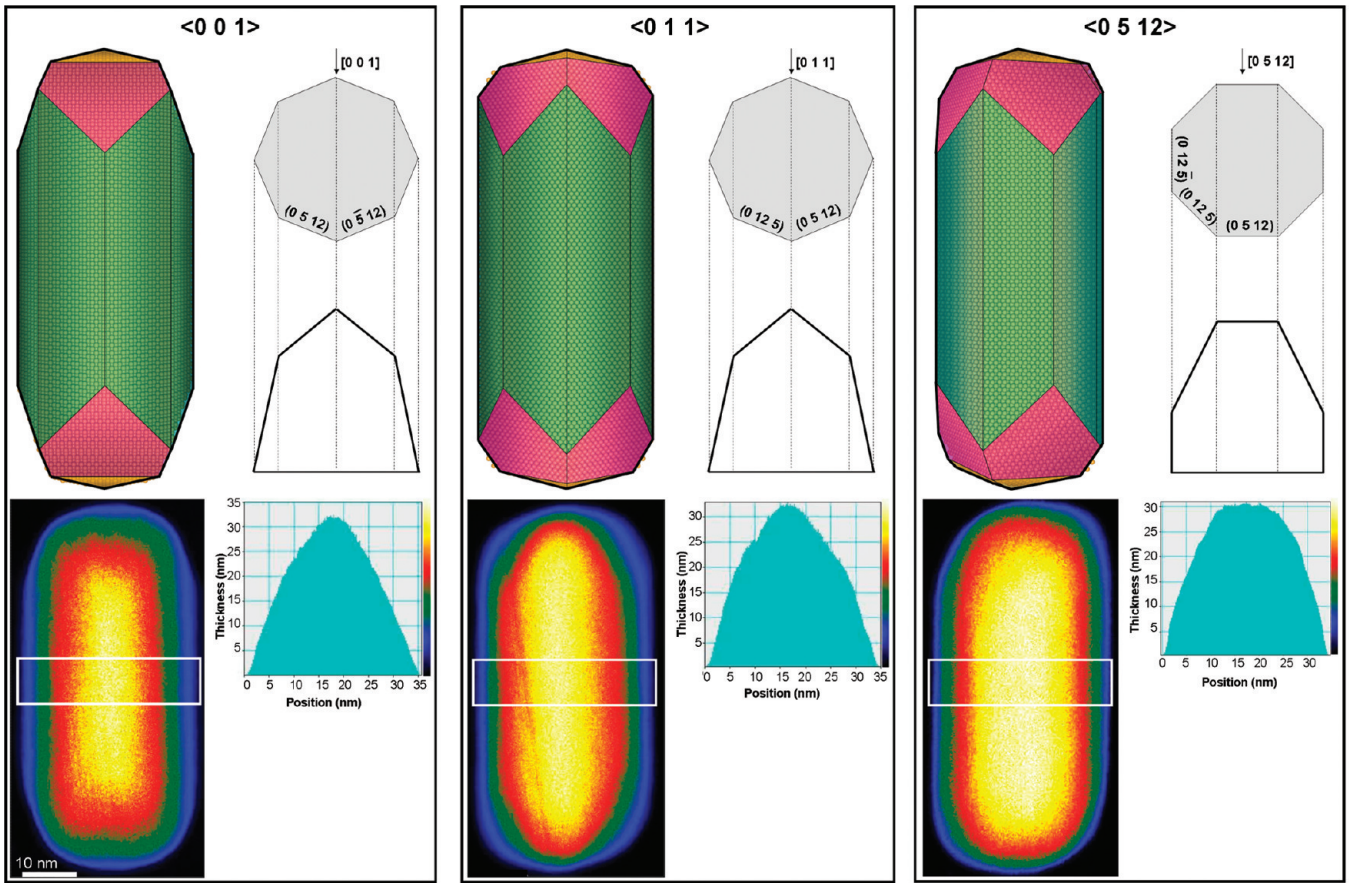

FIGURE 2. Illustration of the determination of the orientation of the facets using the thickness profile method. The top images show the morphology of a nanorod derived from the tomogram in three key zone axes (⟨0 1 1⟩, ⟨0 0 1⟩, and ⟨0 5 12⟩) and the theoretical thickness profile in each orientation (assuming a perfect octagonal cross-section shape). The bottom images show the corresponding experimental thickness-profile image, together with the experimental thickness line profile (averaged over the width of the rectangular region shown). Using this approach, the side-facet orientation was refined and found to lie within 1° of {0 5 12}.

Using this approach, we compare the measured thickness profile with that expected from different orientations of a nanorod of a given shape. The orientation of the nanorod thickness profile can be determined precisely from a convergent-beam electron diffraction pattern recorded at the same time.

Figure 2 illustrates this process and shows the nanorod orientation that best fits the experimental thickness profile for three key zone axes. This confirms that the side facets lie close to the {0 5 12} family of planes, rather than the {0 0 1} or {0 1 1}. To refine the side-facet orientation further, we measured a series of thickness profiles from a given nanorod oriented at 1° intervals from the ⟨0 1 2⟩ to ⟨0 1 3⟩ zone axis. Several nanorods were examined in this detail, and in all cases, we found that the thickness profile with the best fit corresponded to a side-facet orientation perpendicular to ⟨0 5 12⟩. Using this approach, the measurement error could be reduced to 1°. The best fit is readily identified as the profile with the largest region of constant thickness.

We examined over 80 nanorods, and all had thickness profiles consistent with this model, confirming that this morphology is generic. However, we observed that the end-pyramid shape varied from rod to rod, suggesting that the pyramid size and facet orientation may vary.

A model of the shape and the crystallography of the nanorod determined from the tomogram and thickness profiles is displayed in Figure 3 (this model was constructed using VESTA software).[32] For simplicity, this schematic shows equal side lengths and facet angles, although we observed significant variations in both. Furthermore, the intersection between facets is not sharp but rounded, as shown in Figure 1.

It is possible to envisage the crystallographic metamorphosis of a cube into an octagonal rod. The ⟨0 5 12⟩ vector defining the side and bridging facets bisects the ⟨0 0 1⟩ and ⟨0 1 1⟩ directions. An octagonal rod (with {0 5 12} faces) can be built from four sides of a cube (with {0 0 1} faces) using a terraced stack of {0 0 1} atomic planes (Figure 3a,b). This can also be applied to the {0 1 3} pyramid (Figure 3c).

On the atomic scale, the {0 5 12} plane can be thought of as being composed of unit-cell-sized {0 1 2} and {0 1 3} planes (Figure 3b).

It is important to note that the resolution of the tomogram is better than 1 nm but that this is insufficient to resolve

DOI: 10.1021/nl103726k | *Nano Lett.* **2011,** *11,* 273–278

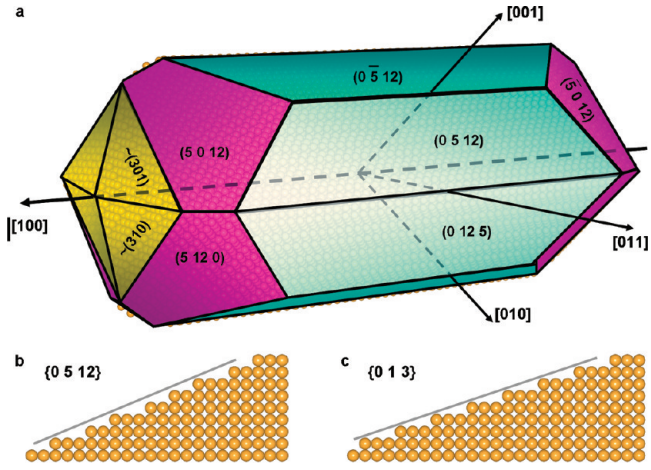

FIGURE 3. (a) Schematic of the gold nanorod morphology. (For simplicity, slight differences in octagonal side lengths and facet angles have been ignored.) The approximately octagonal rod has corner apices that are directed along ⟨0 0 1⟩ or ⟨0 1 1⟩ (in the plane perpendicular to the ⟨1 0 0⟩ long rod axis). The side facets and bridging facets are parallel to the {0 5 12} family of planes (within 1° and 4° measurement error, respectively). The pyramid facets lie within 5° of the {0 1 3} planes but varied slightly from rod to rod. (b, c) Atomic models of the {0 5 12} and {0 1 3} surfaces viewed in the ⟨1 0 0⟩ projection, respectively.

individual atomic steps. Consequently, the question arises as to whether there may be subfacets smaller than 1 nm^2 that are not resolved by the tomogram. The smallest possible {0 1 3} surface viewed in the ⟨1 0 0⟩ projection will be three atoms wide and one atom high (Figure 3c). Similarly, the smallest possible {0 5 12} surface viewed in the ⟨1 0 0⟩ projection will comprise a combination of atomic steps that are two atoms wide and three atoms wide in a sequence (23232) (Figure 3b). Figure 4a shows atomic-resolution HAADF-STEM images of the tip of a gold nanorod taken down the ⟨0 0 1⟩ zone axis, showing the surfaces at atomic resolution in this projection. The atomic-resolution image contrast is clearly consistent with the proposed facet orientation and indicates that the facet persists down to the atomic scale.

We also observed the same nanorod in the ⟨0 1 1⟩ projection (Figure 4b) and again find that the image of the nanorod edge at atomic resolution is consistent with the proposed model viewed in this projection. Note that the shape of the nanorod is such that in this projection the edges of the nanorod correspond to the vector defining the line of intersection between two facets. At the tip, this is the line intersecting two pyramid facets. At the side, this is the line intersecting two bridging facets.

Finally, we note that we also used conventional TEM experiments to confirm that the particles are single crystals, with no evidence of stacking faults, twins, or

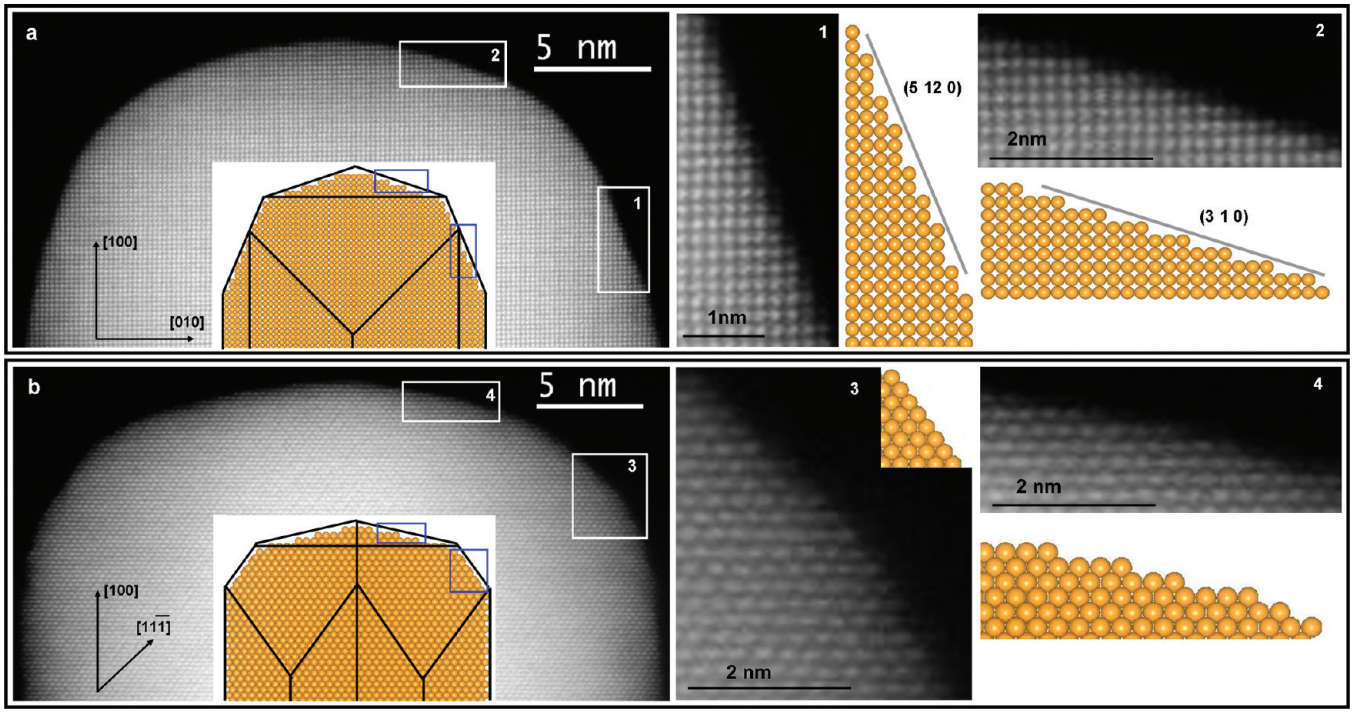

FIGURE 4. Atomic-resolution HAADF-STEM images of the same gold nanorod oriented with the electron beam parallel to the (a) [0 0 1] and (b) [0 1 1] zone axes. The model in Figure 3 is also shown in each projection. Specific parts of the images and the model are extracted and shown at higher magnification in the insets (1−4). Inset 1 shows the (5 12 0) bridging facet in the [0 0 1] projection. Inset 2 shows the (3 1 0) pyramid facet in the [0 0 1] projection. In the [0 1 1] projection, the edges of the nanorod correspond to the vector defining the line of intersection between two facets. Inset 3 shows the edge associated with the intersection of two {0 5 12} bridging facets. Inset 4 shows the edge associated with the intersection of two {3 1 0} pyramid facets. In all cases, the atomic-resolution images are consistent with the model in Figure 3.

DOI: 10.1021/nl103726k | Nano Lett. 2011, 11, 273–278

dislocations. In addition, we found that the nanorods were stable under the electron beam and did not observe any structural rearrangement. Conversely, metal nanocrystals of less than 10 nm^3 in volume (i.e., 2 to 3 orders of magnitude smaller than the nanorods examined here) are well known to be unstable during intense electron beam irradiation.[33−35]

The morphology determined here may explain several apparently anomalous observations regarding nanocrystal growth. Significantly, all of the facets, except the pyramid facets at the rod ends, belong to the same symmetry-equivalent family of planes and will consequently have similar surface energies (unlike the {0 0 1} and {0 1 1} facets previously assumed). This may account for the absence of dendrites along the rods walls. Furthermore, the slightly different orientation of the pyramid facets at the rod ends may explain the promotion of growth along the rod axis and the greater chemical reactivity of the nanorod tips, where oxidation and thiol ligand adsorption selectively occur.[36,37]

The side, bridging, and pyramid facets have intrinsically different sizes, shapes, and hence boundary conditions. This in itself may also affect the growth rates, irrespective of their different orientations.

The fact that the higher-index, sparsely packed {0 5 12} family of facets is so prominent is consistent with the very high affinity of the surfactant for gold surfaces; chemisorption leads to a reduction in the surface free energy and stabilizes the high-index facets, which favors the adsorption of further surfactant. It also indicates that there is strong thermodynamic control of the particle morphology.

In summary, this work has determined, for the first time, the detailed morphology and crystallography of gold nanorods in three dimensions at nanometer resolution, fundamentally revising the current model of morphology and surface crystallography. This is vital for understanding the surface energies of these nanorods. It provides new insights into the growth mechanisms that drive a metal with cubic symmetry to grow into a wide range of morphologies on the nanoscale, with profound implications for controlling their morphology and potentially those of other nanocrystals. In addition, we have demonstrated that the crystallographic orientation of nanorod facets can be determined using a novel method to generate thickness profile images. This provides a valuable and rapid tool for the 3D characterization of nanocrystals. Our results demonstrate that cationic surfactants can significantly reduce the free energy of high-index facets of gold metal, thereby facilitating the formation of new nanocrystal morphologies. Gold nanorods are not simply elongated nanospheres but are fundamentally reconstructed nanocrystals.[38]

Acknowledgment. H.K.-B. thanks Monash University for an MRF Ph.D. scholarship. The data was acquired on instruments within the Monash Centre for Electron Microscopy that were funded by the Australian Research Council (ARC grant LE0454166) and Monash University. A.M.F. acknowledges support from the University of Melbourne Research Office Fellowship. P.M. acknowledges support through ARC grant FF0561486.

Supporting Information Available. The experimental procedure, which includes a description of the specimen preparation method, electron tomography experiments, and the thickness profile method. A movie of the tomogram of a gold nanorod. This material is available free of charge via the Internet at http://pubs.acs.org.

REFERENCES AND NOTES

(1) Balbuena, P. B.; Seminario, J. M. *Nanomaterials: Design and Simulation*; Elsevier: Amsterdam, **2006**.
(2) Woodley, S. M.; Catlow, R. *Nat. Mater.* **2008**, *7*, 937.
(3) Yin, Y.; Alivisatos, A. P. *Nature* **2005**, *437*, 664.
(4) Henry, C. R. *Prog. Surf. Sci.* **2005**, *80*, 92.
(5) Yu, Y.-Y.; Chang, S.-S.; Lee, C.-L.; Wang, C. R. C. *J. Phys. Chem. B* **1997**, *101*, 6661.
(6) Grzelczak, M.; Pérez-Juste, J.; Mulvaney, P.; Liz-Marzán, L. M. *Chem. Soc. Rev.* **2008**, *37*, 1783.
(7) Nikoobakht, B.; El-Sayed, M. A. *Chem. Mater.* **2003**, *15*, 1957.
(8) Xia, Y.; Yang, P.; Sun, Y.; Wu, Y.; Mayers, B.; Gates, B.; Yin, Y.; Kim, F.; Yan, H. *Adv. Mater.* **2003**, *15*, 353.
(9) Zeng, J.; Ma, Y.; Jeong, U.; Xia, Y. *J. Mater. Chem.* **2010**, *20*, 2290.
(10) Nelayah, J.; Kociak, M.; Stephan, O.; Garcia de Abajo, F. J.; Tence, M.; Henrard, L.; Taverna, D.; Pastoriza-Santos, I.; Liz-Marzán, L. M.; Colliex, C. *Nat. Phys.* **2007**, *3*, 348.
(11) Myroshnychenko, V.; Rodríguez-Fernández, J.; Pastoriza-Santos, I.; Funston, A. M.; Novo, C.; Mulvaney, P.; Liz-Marzán, L. M.; de Abajo, F. J. G. *Chem. Soc. Rev.* **2008**, *37*, 1792.
(12) Pérez-Juste, J.; Liz-Marzán, L. M.; Carnie, S.; Chan, D. Y. C.; Mulvaney, P. *Adv. Funct. Mater.* **2004**, *14*, 571.
(13) Gao, J.; Bender, C. M.; Murphy, C. J. *Langmuir* **2003**, *19*, 9065.
(14) Barnard, A. S.; Curtiss, L. A. *J. Mater. Chem.* **2007**, *17*, 3315.
(15) Lofton, C.; Sigmund, W. *Adv. Funct. Mater.* **2005**, *15*, 1197.
(16) Pérez-Juste, J.; Pastoriza-Santos, I.; Liz-Marzán, L. M.; Mulvaney, P. *Coord. Chem. Rev.* **2005**, *249*, 1870.
(17) Carbó-Argibay, E.; Rodríguez-González, B.; Pacifico, J.; Pastoriza-Santos, I.; Pérez-Juste, J.; Liz-Marzán, L. M. *Angew. Chem., Int. Ed.* **2007**, *46*, 8983.
(18) Hee Song, J.; Kim, F.; Kim, D.; Yang, P. *Chem.—Eur. J.* **2005**, *11*, 910.
(19) Wang, Z. L.; Mohamed, M. B.; Link, S.; El-Sayed, M. A. *Surf. Sci.* **1999**, *440*, L809.
(20) Liu, M.; Guyot-Sionnest, P. *J. Phys. Chem. B* **2005**, *109*, 22192.
(21) Keul, H. A.; Möller, M.; Bockstaller, M. R. *Langmuir* **2007**, *23*, 10307.
(22) Buseck, P. R. et al.;. *Proc. Natl. Acad. Sci. U.S.A.* **2001**, *98*, 13490.
(23) Henglein, A.; Giersig, M. *J. Phys. Chem. B* **1999**, *103*, 9533.
(24) Midgley, P. A.; Weyland, M. *Ultramicroscopy* **2003**, *96*, 413.
(25) Katz-Boon, H. A Method for the Characterisation of Gold Nano-Rods. Ph.D. thesis; Monash University, Melbourne, Australia, 2010.
(26) Hillyard, S.; Loane, R. F.; Silcox, J. *Ultramicroscopy* **1993**, *49*, 14.
(27) Dwyer, C.; Etheridge, J. *Ultramicroscopy* **2003**, *96*, 343.
(28) Treacy, M. M. J.; Gibson, J. M. *Ultramicroscopy* **1993**, *52*, 31.
(29) Allen, L. J.; Findlay, S. D.; Oxley, M. P.; Rossouw, C. J. *Ultramicroscopy* **2003**, *96*, 47.
(30) http://www.mcem.monash.edu.au/facilities/newbuilding.html.
(31) Midgley, P. A.; Weyland, M.; Yates, T. J. V.; Arslan, I.; Dunin-Borkowski, R. E.; Thomas, J. M. *J. Microsc.* **2006**, *223*, 185.
(32) Momma, K.; Izumi, F. *J. Appl. Crystallogr.* **2008**, *41*, 653.
(33) Li, Z. Y.; Young, N. P.; Di Vece, M.; Palomba, S.; Palmer, R. E.; Bleloch, A. L.; Curley, B. C.; Johnston, R. L.; Jiang, J.; Yuan, J. *Nature* **2008**, *451*, 46.
(34) Iijima, S.; Ichihashi, T. *Phys. Rev. Lett.* **1986**, *56*, 616.

DOI: 10.1021/nl103726k | *Nano Lett.* **2011,** *11,* 273–278

(35) Ajayan, P. M.; Marks, L. D. *Phys. Rev. Lett.* **1989**, *63*, 279.
(36) Rodríguez-Fernández, J.; Pérez-Juste, J.; Mulvaney, P.; Liz-Marzán, L. M. *J. Phys. Chem. B* **2005**, *109*, 14257.
(37) Thomas, K. G.; Barazzouk, S.; Ipe, B. I.; Joseph, S. T. S.; Kamat, P. V. *J. Phys Chem B* **2004**, *108*, 13066.
(38) During the processing of this manuscript, a related paper has been brought to our attention, which is in close agreement with our main conclusions: Carbó-Argibay, E.; Rodríguez-González, B.; Gómez-Graña, S.; Guerrero-Martínez, A.; Pastoriza-Santos, I.; Pérez-Juste, J.; Liz-Marzán, L. M. *Angew. Chem. Int. Ed.* **2010**, *49*, 9397.
(39) Gilbert, P. *J. Theor. Biol.* **1972**, *36*, 105.
(40) http://www.amira.com/.
(41) Rossouw, C. J. *Ultramicroscopy* **1995**, *58*, 211.
(42) Rossouw, C. J.; Allen, L. J.; Findlay, S. D.; Oxley, M. P. *Ultramicroscopy* **2003**, *96*, 299.

DOI: 10.1021/nl103726k | *Nano Lett.* **2011,** *11,* 273–278